DOI 10.5012/bkcs.2010.31.5.1241

The Importance of the Aging Time to Prepare $Cu/ZnO/Al_2O_3$ Catalyst with High Surface Area in Methanol Synthesis

Heon Jung, Dae-Ryook Yang, Oh-Shim Joo,[†] and Kwang-Deog Jung[†,*]

Department of Chemical & Biological Engineering, Korea University, Anam-dong, Seongbuk-gu, Seoul 136-701, Korea
[†]Clean Energy Research Center, Korea Institute of Science and Technology, P.O. Box 131, Cheongryang, Seoul 136-791, Korea. [*]E-mail: jkdcat@kist.re.kr
Received February 7, 2010, Accepted March 8, 2010

Ternary $Cu/ZnO/Al_2O_3$ catalysts were prepared by a co-precipitation method. The precursor structures were monitored during the aging. The first precipitate structure was amorphous georgeite, which transformed into the unknown crystalline structure. The transition crystalline structure was assigned to the crystalline georgeite, which was suggested with elemental analysis, IR and XRD. The final structure of precursors was malachite. The Cu surface area of the resulting $Cu/ZnO/Al_2O_3$ was maximized to be 30.6 m^2/g at the aging time of 36 h. The further aging rapidly decreased Cu surface areas of $Cu/ZnO/Al_2O_3$. ZnO characteristic peaks in oxide samples almost disappeared after 24 h aging, indicating that ZnO was dispersed in around bulk CuO. TOF of the prepared catalysts of the Cu surface area ranges from 13.0 to 30.6 m^2/g_{cat} was to be 2.67 ± 0.27 mmol/m^2.h in methanol synthesis at the condition of 250 °C, 50 atm and 12,000 mL/g_{cat}. h irrespective of the XRD and TPR patterns of CuO and ZnO structure in $CuO/ZnO/Al_2O_3$. The pH of the precipitate solution during the aging time can be maintained at 7 by CO_2 bubbling into the precipitate solution. Then, the decrease of Cu surface area by a long aging time can be prevented and minimize the aging time to get the highest Cu surface area.

Key Words: Methanol synthesis, $Cu/ZnO/Al_2O_3$ catalyst, Malachite, Georgeite, Aging time

Introduction

Methanol synthesis is focused by recent interests on methanol economy[1] and methanol utilizations such as MTO (methanol to olefin)[2-3] and bio-disel. $Cu/ZnO/Al_2O_3$ catalytic system has been used for commercial methanol synthesis. However, the active origins of Cu/ZnO interaction have been studied for the last decade. One of the controversial issues was which one of CO and CO_2 was the key reactant for methanol synthesis. CO had been regarded as a key reactant for methanol synthesis. Kagan *et al*.[4-5] claimed that CO_2 was the key reactant for methanol synthesis, but it was not accepted until it was proposed by Chinchen *et al.*[6] In that point of view, many kinetic equations were presented based on CO[7-8] or CO_2[9-10] or both CO and CO_2[11-12] as the reactant in methanol synthesis. Another controversial issue was which one of Cu^{+1} and Cu was the active center for methanol synthesis. Klier *et al.*[11] suggested that the reduction of Cu^{+1} during the reaction would be the cause of deactivation. However, the direct correlation between Cu^{+1} concentration and the activity was not shown, although the importance of Cu^{+1} was emphasized by several authors.[13-14] On the other hand, the structure sensitivity of Cu based catalysts has been the other important issue. It was claimed that the methanol synthesis was structure-insensitive by showing that methanol synthesis rates were linearly proportional to Cu surface areas using $Cu/ZnO/Al_2O_3$, Cu/SiO_2 and Cu/MgO.[15] On the other hand, it was suggested that the methanol synthesis rates were maximized with Cu/ZnO catalytic systems, emphasizing that ZnO played the key role in methanol synthesis, that is, transport phenomena of one adsorbed species.[16] The view suggested that it was hydrogen atoms which migrated from Cu to ZnO, the latter acting as a sink for the hydrogen atoms for their ready transference back to Cu to hydrogenate the formate species to methanol.[17]

On the other hand, the formate species[18] and hydrogen spillover[19-20] from Cu to ZnO and ZrO_2 were also observed and it was suggested that the formate species were hydrogenated on ZnO and ZrO_2. Although there were controversial on the promotional effects of ZnO, it was clearly shown that apparent methanol synthesis rates increased with an increase in Cu surface areas even in the case of the structure-sensitive Cu based catalysts on methanol synthesis.[21-22] Therefore, the importance of Cu surface area cannot be overemphasized in the practical aspect. It has been discussed that the structures of the precursors were related to the final activity of the resulting $Cu/ZnO/Al_2O_3$ catalysts. Klier *et al*.[11] observed the hydroxynitrate, the zinc hydroxycarbonate and the mixed copper zinc hydroxy carbonate. According to their results, the precursor structures changed with the ratios of Cu/Zn and the catalyst from the mixed copper zinc hydroxy carbonate (aurichalcite) showed the highest activity. On the other hand, Hoppener *et al*.[12] prepared a single phase rosasite precursor and the catalyst from that precursor showed the highest activity. Fujita *et al*.[24] prepared the malachite, aurichalcite and hydrozincite depending on the ratios of Cu/Zn and concluded that the activity of the catalyst from aurichalcite showed higher than that from malachite or zinc hydrozincite. During the catalyst preparation, the structural transformation of the precursor was monitored during the long term aging time and that the Cu surface areas of the resulting oxide samples were optimized during the aging. It was shown that the specific activity of the prepared catalysts increased with an increase in the specific Cu surface area.

Experimental

Preparation of the catalyst. The precursors of methanol synthesis catalysts with the mol ratio of Cu : Zn : Al = 6 : 3 : 1 were

prepared by a co-precipitation method from their nitrates solution at a pH ~7.0. Buffer solution of a pH 8 containing a mixture of $NaHCO_3$ and Na_2CO_3 were used as the precipitation agents throughout the works.

In a typical catalyst preparation, $Cu(NO_3)_2{\cdot}3H_2O$, $Zn(NO_3)_2{\cdot}6H_2O$, and $Al(NO_3){\cdot}9H_2O$ were dissolved in H_2O to get 0.3 M of metal nitrate solution. The buffer solution was added into a solution of metal nitrates under vigorous agitation at room temperature and the initial pH of the slurry was to be in a range from 7.0 to 7.5. The precipitates was filtered and washed with distilled water after the aging for 0, 6, 12, 18, 24, 48, and 72 h at room temperature.

The washed samples were dried in a vacuum oven for 24 hours at 100 °C. The resulting dried samples were calcined at 450 °C for 6 hours. The catalysts with the different aging time were designated as CZA (aging time in h).

Characterization of the catalyst. Chemical compositions of the precursors were analyzed by an atomic absorption spectroscopy (UNICAM M-series), ICP (Varian 710-ES, 1.3 kW) and CHN analysis (FISONS Instrument Version 2A1108).

Crystal structures of samples were identified by a powder X-ray diffraction spectroscopy (Shimadzu 6000, Cu Kα radiation, 40 kV, 30 mA). BET surface areas of samples were obtained using a Micromeritics ASAP 2000 instrument. Reducibility of the oxide catalysts was measured by the H_2-temperature-programmed reduction (H_2-TPR) experiments using Catalyst Analyzer BELCAT-B model. In a typical H_2-TPR experiment, a catalyst sample of about 30 mg was used. This sample was heated in a stream of 5 vol% H_2 in Ar (20 mL/min) with a heating rate of 10 °C /min up to 600 °C and maintained at 600 °C for 30 min. Cu surface areas, S_{cu}, were determined by a N_2O titration. Porapak N column was used for the N_2O and N_2 separation. For an example, 40 mg of sample was loaded and reduced using 5 vol % H_2 in Ar at 250 °C for 2 h and the reactor was purged in a He stream (99.999 %) with a de-oxo unit at 150 °C for 30 min and cooled down to 90 °C, and then, the N_2O titration was carried out. A surface copper density of 1.47×10^{19} atoms/m^2 assuming Cu : O = 2 : 1 was used for the calculation of Cu surface areas. As a reference, M-54 (I.C.I.) catalyst was used.

Catalytic reaction. Catalytic activity measurements were carried out in a fixed-bed tubular reactor (i.d.: 3/8 in.). The products were analyzed using an on-line gas chromatograph equipped with a thermal conductivity detector (TCD). For methanol synthesis, the prepared catalysts were pre-reduced in a 5% H_2/N_2 gas at 250 °C for 5 h. After the reduction, the feed gases (the molar ratio of $CO:CO_2:H_2$ = 1:4:16) was introduced into the reactor at the pressure of 50 atm, a GHSV of 12,000 mL/g_{cat} h and the temperature range of 240 to 270 °C. Turnover Frequency (TOF) in the methanol synthesis was defined as the methanol production rates per Cu surface area of catalyst used in mmol/m^2. h.

Result and Discussion

Table 1 shows the results of the elemental analysis of the CZA precursors with the different aging time. Nitrogen amount was negligible by CHN analysis in the all precursors. Assuming that Al component is in the form of $Al(OH)_3$, all the precursors with the different aging time have the same chemical composition of $Cu_{1.4}Zn_{0.6}(OH)_2CO_3$, indicating that the chemical composition does not change during the aging. It is plausible that hydroxynitrate forms at the initial stage, but the precursor of CZA (0) shows the hydroxycarbonate only, indicating that the transformation rate from hydroxynitrate to hydroxycarbonate is so fast. Figure 1 shows XRD patterns of CZA precursors with the different aging time. The amorphous structure of CZA (0) with the chemical composition of $Cu_{1.4}Zn_{0.6}(OH)_2CO_3$ can be assigned to georgeite.[25] The georgeite was crystallined after 6 h aging. The structure of CZA (6) and CZA (12) has the characteristic peaks at 12.9, 18.3, 22.6, 26.2, 32.0, and 37.1°. This kind of XRD pattern is not be found in JCPDS cards. Therefore, the structure is assigned to the crystalline georgeite, tentatively, because it has the same chemical composition with the georgeite and the different patterns from other precursors such as malachite, aurichalcite, and azurite. The crystalline georgeite, tentatively assigned, is reported first time and observed during the structural transition from the amorphous georgeite to malachite. The structure of samples after the further aging can be assigned to malachite (JCPDS 75-1163). It is interesting to note that the width of the lines is broadened, indicating the crystal sizes became smaller during the aging. For the confirmation of the precursor structures, IR spectra of the precursors were taken to monitor carbonate and hydroxide.

Figure 2 shows IR spectra of the eight samples with the different aging times. The precursors of CZA (0), CZA (6) and CZA (12) show the same IR spectra, although the precursor of

Table 1. Elemental analysis and chemical compositions of the prepared precursors.

Catalysts	Elemental Analysis (wt %)						Chemical compositions of Cu/Zn hydroxy carbonate
	Cu	Zn	Al	$C(CO_3)$	$H((OH)_2)$	Total	
CZA(0)	33.6	13.8	2.1	4.6 (23.0)	1.8 (30.6)	103.1	$Cu_{1.4}Zn_{0.6}(OH)_{2.3}(CO_3)_{1.0}$
CZA(6)	33.2	13.8	2.1	4.4 (22.0)	1.7 (29.9)	100.0	$Cu_{1.4}Zn_{0.6}(OH)_{2.2}(CO_3)_{1.0}$
CZA(12)	31.1	13.8	2.2	4.3 (21.5)	1.5 (25.5)	94.1	$Cu_{1.4}Zn_{0.6}(OH)_{1.8}(CO_3)_{1.0}$
CZA(18)	33.5	14.4	2.1	4.2 (21.0)	1.6 (27.2)	98.2	$Cu_{1.4}Zn_{0.6}(OH)_{2.0}(CO_3)_{0.9}$
CZA(24)	32.8	14.4	2.1	4.5 (22.5)	1.7 (28.9)	100.7	$Cu_{1.4}Zn_{0.6}(OH)_{2.2}(CO_3)_{1.0}$
CZA(36)	33.4	14.5	2.1	4.4 (22.0)	1.7 (28.9)	100.9	$Cu_{1.4}Zn_{0.6}(OH)_{2.2}(CO_3)_{1.0}$
CZA(42)	34.1	14.9	2.1	4.5 (22.5)	1.7 (28.9)	102.5	$Cu_{1.4}Zn_{0.6}(OH)_{2.4}(CO_3)_{1.0}$
CZA(72)	34.1	14.7	2.1	4.6 (23.0)	1.8 (30.6)	104.4	$Cu_{1.4}Zn_{0.6}(OH)_{2.4}(CO_3)_{1.0}$

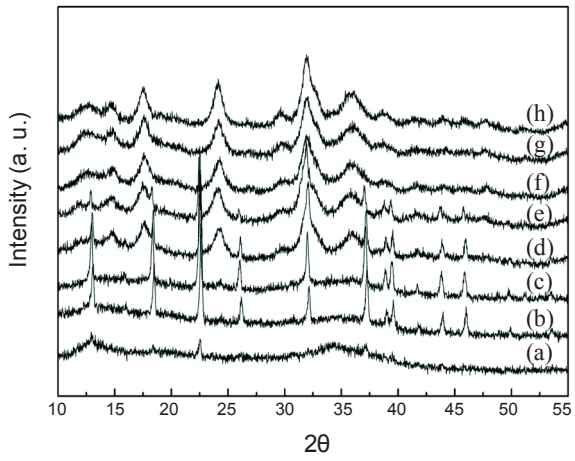

Figure 1. XRD patterns of the prepared precursors: (a) CZA (0), (b) CZA (6), (c) CZA (12), (d) CZA (18), (e) CZA (24), (f) CZA (36), (g) CZA (48), and (h) CZA (72).

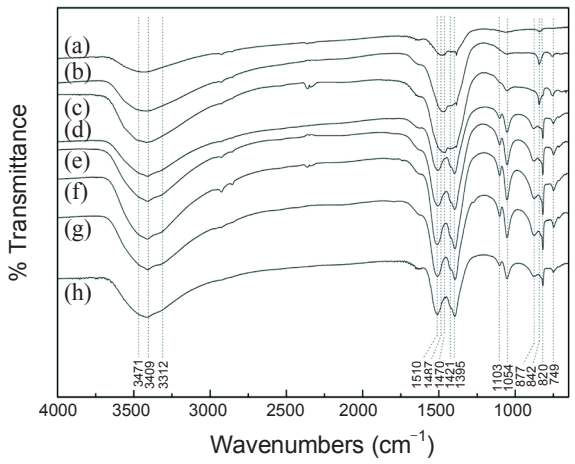

Figure 2. IR Spectra of the eight samples with the different aging time: (a) CZA (0), (b) CZA (6), (c) CZA (12), (d) CZA (18), (e) CZA (24), (f) CZA (36), (g) CZA (48), and (h) CZA (72).

CZA (0) has the amorphous structure differently from the precursors of CZA (6) and CZA (12). That indicates that M-OH and M-CO_3 bonding strengths and configurations are not different each other, supporting that CZA (6) and CZA (12) can be the crystalline georgeite. The IR spectra of CZA (0) are coincided with those of georgeite.[26] All the precursors after 24 h aging show the same IR spectra. Bands at 3471, 3409 and 3312 cm^{-1} were observed for the OH species. Bands at 3317 and 3412 cm^{-1} can be assigned to OH stretching modes of two crystallographically different OH^- ions in the pure malachite crystal lattice.[27-28] However, it should be noted that another peak at 3471 cm^{-1} was not only observed, but the peaks became also broad as compared with the pure malachite which has the well defined separate peaks at 3409 and 3312 cm^{-1}. The absorption bands of OH ions became broad when Zn was added into the malachite structure and the shoulder peak at 3471 cm^{-1} was observed with the composition of $Cu_xZn_{2-x}(OH)_2CO_3$, supporting the results of the elemental analysis[27]. Bands at 877, 1054 and 1103 cm^{-1} can be assigned to M-OH bending modes. On the other hand, the carbonate ν_1 mode will appear at 1085 cm^{-1} and the corresponding band overlaps with that of the M-OH bending mode.[28-29] The peaks at 1421, 1470, 1510, and 1520 cm^{-1} (shoulder) can be assigned to the carbonate asymmetric stretching vibrational mode (ν_3). The bands of carbonate ν_3 mode of pure malachite were observed at 1395, 1430, 1500 and 1519 cm^{-1} and the shifts of ν_3 bands of the samples (d)-(g) indicate that Zn^{+2} ions are included in the mala-

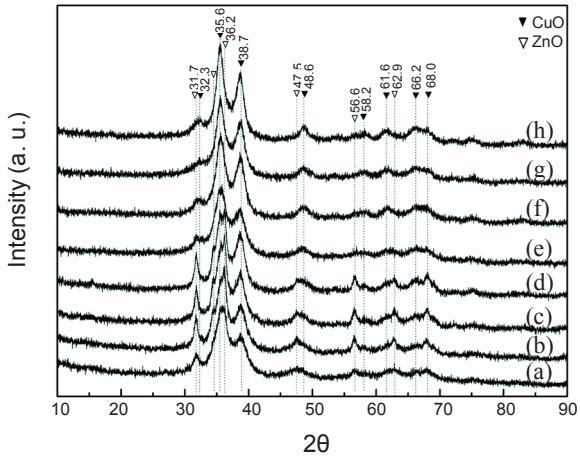

Figure 3. XRD patterns of the prepared oxide catalysts: (a) CZA (0), (b) CZA (6), (c) CZA (12), (d) CZA (18), (e) CZA (24), (f) CZA (36), (g) CZA (48), and (h) CZA (72).

Table 2. Physical properties and activity of methanol synthesis of the prepared CZA catalysts.

Catalysts	S_{BET} (m^2/g)	Pore volume (cc/g)	Cu surface area (m^2/g)	Methanol yield (%) at 250 °C	TOF at 250 °C (mmol/m^2.h)*
CZA (0)	111.4	0.58	10.5		
CZA (6)	101.9	0.57	10.6	12.7	2.01
CZA (12)	103.1	0.62	13.0	20.2	2.61
CZA (18)	111.4	0.45	22.6	35.6	2.64
CZA (24)	132.5	0.48	27.9	40.1	2.41
CZA (36)	201.2	0.65	30.6	49.7	2.72
CZA (42)	170.4	0.56	27.7	43.3	2.62
CZA (72)	131.6	0.59	21.9	36.5	2.79
M-54	-	-	22.6	39.8	2.95

*TOF was obtained at the reaction conditions of 250 °C, 50 atm and 12,000 mL/g_{cat}.h.

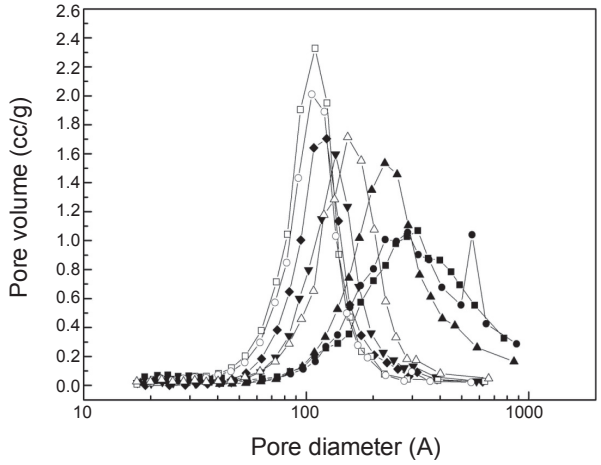

Figure 4. Pore size distributions of the prepared oxide catalysts: –■– CZA (0), –●– CZA (6), –▲– CZA (12), –▼– CZA (18), –◆– CZA (24), –□– CZA (36), –○– CZA (48), –△– CZA (72).

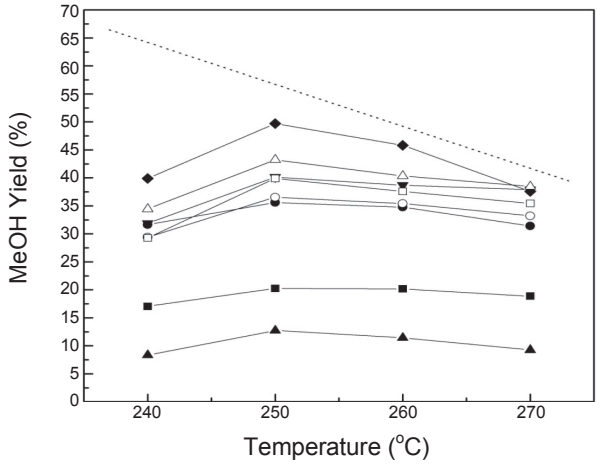

Figure 6. Methanol yields of CZA catalysts with respect to the reaction temperature at 250 °C, 50 atm and 12,000 mL/g_{cat}.h: –▲– CZA (6), –■– CZA (12), –●– CZA (18), –▼– CZA (24), –◆– CZA (36), –△– CZA (48), –○– CZA (72), –□– M-54.

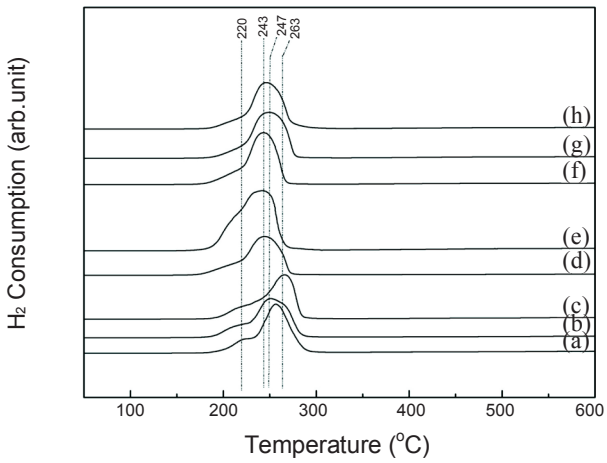

Figure 5. H_2-TPR analysis of the prepared oxide samples: (a) CZA (0), (b) CZA (6), (c) CZA (12), (d) CZA (18), (e) CZA (24), (f) CZA (36), (g) CZA (48), and (h) CZA (72).

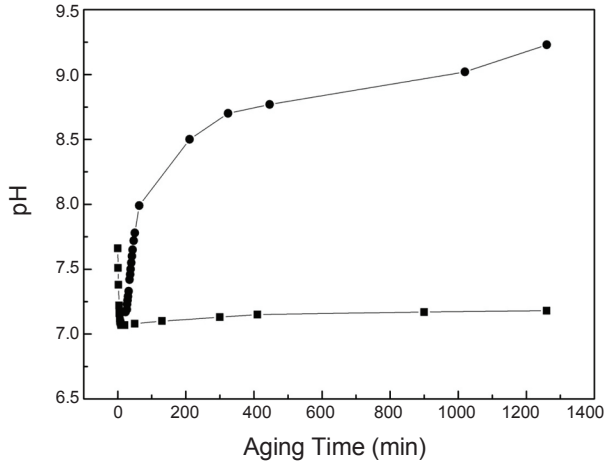

Figure 7. The pH changes of the precipitate solution during the aging: –●– No CO_2 purge, –■– CO_2 purge.

chite lattice.[28] The sharp band at 820 cm^{-1} with a shoulder are assigned to the carbonate out-of-plane bending mode (ν_2) and the band at 749 cm^{-1} with shoulders can be assigned to the carbonate in-plane bending mode (ν_4).

However, it was observed that the absorption bands of carbonate ions in malachite were not different from monophasic mixed Cu-Zn hydroxycarbonate upto 20% Zn content.[28]

Figure 3 shows XRD patterns of oxide samples prepared from the eight precursors. The precursors were calcined at 450 °C for 6h. The XRD pattern from the amorphous precursor of CZA (0) shows both CuO and ZnO at 35.6 and 36.2°, respectively. The XRD patterns from the precursors of CZA (6) and CZA (12) with the high crystallinity show that the intensity of the peak at 36.2° (ZnO) is stronger than that at 35.6° (CuO). The XRD patterns from the precursors after the 24 h aging show that ZnO peaks are minimized and the peak at 35.6° (CuO) is shown mainly. The peak at 31.7° shows changes of ZnO crystallinity in the metal oxides with the aging time, clearly. The oxide samples from the crystalline georgeite show the high crystallinity of ZnO, as compared with those from the malachite. ZnO crystalline phases are minimized in the oxide samples from malachite precursors, indicating that ZnO particle sizes are too small to be observed in XRD. Therefore, it can be deduced from the XRD patterns that ZnO is well dispersed in around CuO.

Table 2 shows the Cu and BET surface areas with the respect to the aging time. The Cu surface area was maximized to be 30.6 m^2/g_{cat} at 36 h aging time and rather decreased with the further aging, although both XRD patterns and IR spectra did not show any distinctive changes of the characteristic peaks after 36 h aging. It should be noted that the Cu surface areas increased with an increase in BET surface areas, indicating that the prepared catalysts were homogeneous. The Cu surface areas rapidly decrease after 36 h aging. So, the importance of the aging time should be emphasized for the preparation of $Cu/ZnO/Al_2O_3$

catalysts. Previously, the precursor effects were emphasized to get the high active methanol synthesis catalysts. In that point of view, one of the precursors among the malachite, aurichalcite, and rosasite was preferred for methanol synthesis by several authors.[11,23-24] However, it should be clarified that the aging time should be optimized on each precursor before the effects of precursors were investigated.

Figure 4 shows the pore size distribution of the oxide samples. The pore volume was maximized and the pore diameter was minimized at 36 aging time. The pore diameter increased with the aging time after the 36 h aging. The pore size analysis indicates that the changes of BET surface areas are closely related to the pore size distribution. Therefore, the decrease of Cu surface areas after 36 h aging cannot be attributed to the modification of the structure between Cu and ZnO, but to a decrease in BET surface areas resulted from the changes of the pore size distribution.

Figure 5 shows the TPR patterns of the oxide samples. TPR patterns of CuO can be described in the points of view of the crystallinity and the valence state changes. The reduction peaks of CZA (0) from the amorphous geogeite were observed at 220 and 255 ^{o}C. The reduction peak at 255 ^{o}C was split into two peaks at 247 and 263 ^{o}C with CZA(6h) and further at 240 and 265 ^{o}C. The reduction peaks of oxide samples from the malachite structure were observed at 243 ^{o}C with the shoulder and the reduction peak at 240 ^{o}C was broadened after 36 h aging. The peak at the temperature lower than 220 ^{o}C can be ascribed to the dispersed CuO. The reduction temperature at about 220 ^{o}C decreased with the aging time. The reduction peak at the temperature higher than 220 ^{o}C can be attributed to the reduction of the bulk CuO and the shoulder peaks can be due to the stepwise reduction of $Cu^{+2} \rightarrow Cu^{+1} \rightarrow Cu^{o}$. XRD patterns of CZA (6) and CZA (12) show the distinctive CuO and ZnO, while those of oxide samples after 18 h aging show that ZnO is dispersed around CuO from XRD patterns. From TPR patterns, it indicates that the high reduction temperature of CZA (6) and CZA (12) can be ascribed to the bulk CuO with low interaction with ZnO, while the low reduction temperature of CZA from malachite can be due to the bulk CuO in the dispersed ZnO phase.

Figure 6 shows the methanol yields with respect to the reaction temperature with the eight $Cu/ZnO/Al_2O_3$ samples. The M-54 catalyst (I.C.I.) was used as a reference. The Cu surface area of M-54 was 22.6 m^2/g_{cat} in this N_2O titration experimental condition. Methanol synthesis was conducted at the condition of 250 ^{o}C, 50 atm and 12,000 mL/g_{cat}.h to correlate the Cu surface areas with methanol yields.

As expected, the CZA (36) with the highest Cu surface area shows the highest methanol yield. Both CZA (36) and CZA (48) approached to the equilibrium conversion at 270 ^{o}C. Methanol yields on CZA (18) with the Cu surface area of 22.6 m^2/g_{cat} and CZA (72) with the Cu surface area of 21.9 m^2/g_{cat} (similar to M-54) were slightly lower than those on M-54 as shown in Table 2. If the methanol production rates are plotted with the specific Cu surface areas, it is clear that the methanol yields increase with an increase of Cu surface area within the allowable deviation (2.67 ± 0.27 mmol/m^2.h) (The TOF of CAZ (6) was excluded in the allowable deviation calculation). TOF of CZA (6) shows the lowest value of 2.01 mmol/m^2.h, while M-54 shows the highest TOF of 2.95 mmol/m^2.h. TOF of CZA (12) is not different from ones of CZA catalysts from malachite, which indicates that the interfacial role between CuO and ZnO is not so crucial in methanol synthesis, but that the first importance should be given on the surface areas of Cu.

Figure 7 shows the pH changes with the aging time. It was reported that the percentage precipitated of Cu, Zn and Al was different depending on pH of precipitation,[30] but Table 1 and Figure 6 indicate that the composition of the precipitate do not change with the pH of the precipitate solution. Therefore, the increase of pH of the solution can be due to the evolution of CO_2 into the air. CO_2 gas was introduced into the solution to adjust the pH of the solution to 7.0 during the aging as shown in Fig 7. In that case, the georgeite disappeared and transformed into malachite structure within 6 h. The Cu surface areas of CZA (12) and CZA (24) with CO_2 bubbling was 32.3 m^2/g_{cat} and 35.4 m^2/g_{cat}. The decrease of Cu surface areas was not observed even after 72 h aging, indicating that the decrease of CZA for the long aging time can be prevented by maintain the pH of the precipitate solution at pH 7.

Conclusion

During the aging after the co-precipatiation at pH 7, the amorphous geogeite appeared at 0 h aging and transformed into the unknown crystalline structure at 6 and 12 h aging, which was assigned to the crystalline georgeite by elemental analysis, XRD and IR. The crystalline geogeite transformed into malachite structure at 18 h aging. XRD patterns of oxide samples showed the distinctive CuO and ZnO characteristic peaks at 6, 12, and 18 h aging. The malachite structure was maintained during the further aging, but the distinctive ZnO patterns of oxide samples almost disappeared. The Cu surface area was maximized to be 30.6 m^2/g_{cat} at 36 h aging time and rapidly decreased with the further aging. Although XRD and TPR patterns of CZA (12), CZA (18) and CZA (24) were quite different each other, TOF of each sample was 2.60, 2.63, and 2.41 g/m^2.h at 250 ^{o}C, 50 atm and 12,000 mL/gcat.h, irrespective of the structural differences. TOF of the eight samples including the commercial M-54 catalyst (ICI) was within 2.67 ± 0.27 mmol/m^2.h. The pH of the precipitate solution during the aging time can be maintained at 7 by CO_2 bubbling into the precipitate solution. Then, the decrease of Cu surface area by long time aging can be prevented and minimize the aging time to get the highest Cu surface area.

References

1. Olah, G. A.; Geoppert, A.; Prakashi, G. K. S. *Beyond Oil and Gas: The Methanol Economy*; Wiley-Vch: USA, 2006
2. Stocker, M. *Microporous Materials* **1999**, *29*, 3.
3. Song, W.; Marcus, D. M.; Fu, H.; Ehresmann, J. O.; Haw, J. F. *J. Am. Chem. Soc*. **2002**, *124*, 3844.
4. Kagan, Y. B.; Liberov, L. G.; Slivinsky, E. V.; Lockev, S. M.; Lin, G. I.; Rozovsky, A. Y.; Bashkirov, A. N. *Dokl. Alcad. Nauk*, SSSR. **1975**, *222*, 1093.
5. Rozovskii, A. Ya.; Lin, G.; Liberov, L. B.; Slivinskii, E. V.; Loktev, S. M.; Kagan, U. B.; Bashkirov, A. N. *Kinetics and Catalysis* **1997**, *18*, 691.
6. Chinchen, G. C.; Denny, P. J.; Parker, D. G.; Spencer, M. S.; Whan, D. A. *Appl. Catal*. **1987**, *30*, 333.

7. Leonov, V. E.; Karavaev, M. M.; Tsybina, E. N.; Pertrischeva, G. S. *Kinet. Katal*. **1973**, *14*, 848.
8. Villa, P.; Forzatti, P.; Buzzi-Ferraris, G.; Garone, G.; Pasquon, I. *Ind. Eng. Chem. Proc. Des. Dev*. **1985**, *24*, 12.
9. Skrzypek, J.; Lachowska, M.; Grzesik, M.; Sloczynski, J.; Nowak, P. *Chem. Eng. J*. **1995**, *58*, 101.
10. Bussche, K. M. V.: Froment, G. F. *J. Catal*. **1961**, *161*, 1.
11. Klier, K.; Chatikavanij, V.; Herman, R. G.; Simmons, G. W. *J. Catal*. **1982**, *74*, 343.
12. Graaf, G. H.; Scholtens, H. Stamhuis, E. J.; Beenackers, A.A.C.M. *Chem. Eng. Sci*. **1990**, *45*(4), 773.
13. Klier, K. *Adv. Catal*. **1982**, *31*, 243.
14. Szanyi, J.; Goodman, D.W. *Catal. Lett*. **1991**, *10*, 383.
15. Chinchen, G. C.; Waugh, K. C.; Whan, D. A. *Appl. Catal*. **1986**, *25*, 101.
16. Burch, R.; Chappell, R. J.; Golunski, S. E. *Catal. Lett*. **1988**, *1*, 439.
17. Spencer, M. S.; Burch, R.; Golunski, S. E. *J. Chem. Soc. Faraday Trans*. **1991**, *87*, 1791.
18. Joo, O. S.; Jung, K. D.; Han, S.; Uhm, S.; Lee, D.; Ihm, S. *Appl. Catal*. **1996**, *35*, 273.
19. Fisher, I. A.; Bell, A. T. *J. Catal*. **1998**, *172*, 153.
20. Jung, K. D.; Bell, A. T. *J. Catal*. **2000**, *193*, 207.
21. Joo, O. S.; Jung, K. D.; Han, S.; Uhm, S. *Int. Symposium on CO_2 Chemistry* **1993**, 93.
22. Venugopal, A.; Palgunadi, J.; Jung, K. D.; Joo, O. S.; Shin, C. *J. Mol. Catal*. **2009**, *302*, 20.
23. Hoppener, R. H.; Doesburg, E. B. M.; Scholten, J. J. F. *Appl. Catal*. **1985**, *25*,109.
24. Fujita, S.; Kanamori, Y.; Satriyo, A. M.; Takezawa, N. *Catal. Today* **1998**, *45*, 241.
25. Spenser, M. S. *Catal. Lett*. **2000**, *66*(4), 255.
26. Pollard, A. M.; Spenser, M. S.; Thomass, R. G.; Williams, P. A. *Appl. Catal. A* **1992**, *85*, 1.
27. Xu. J.; Xue, D. *J. Phys. Chem. B* **2005**, *109*, 17157.
28. Stoilova, D.; Koleva, V.; Vassileva, V. *Spectrochimca Acta A* **2002**, *58*, 2051.
29. Frost, R. L.; Martens, W. N.; Rintoul, L.; Mahmutagic, E.; Kloprogge, J. T. *J. Raman Spectrosc*. **2002**, *33*, 252.